



DESIGN AND CONSTRUCTION OF A FRICTION WELDING EQUIPMENT WITH LASER ASSISTANCE FOR THE JOINT OF AISI 1045 STEEL AND ALUMINUM 2017-T4 SHAFTS

DISEÑO Y CONSTRUCCIÓN DE UN EQUIPO DE SOLDADURA POR FRICCIÓN CON ASISTENCIA LÁSER PARA LA UNIÓN DE EJES DE ACERO AISI 1045 Y ALUMINIO 2017-T4

José Luis Mollo^{1,2} , Jorge Andrés Ramos-Grez^{1,3} ,

Germán Omar Barrionuevo^{1,*}

Received: 17-04-2021, Received after review: 12-08-2021, Accepted: 02-09-2021, Published: 01-01-2022

Abstract

Welding metal alloys with dissimilar melting points make conventional welding processes unfeasible to be used. On the other hand, friction welding has proven to be a promising technology capable of joining materials, while preventing the temperature from exceeding the melting point. However, obtaining a welded joint with mechanical properties that are similar to the base materials remains a challenge. In the development of this work, a laser-assisted rotary friction welding equipment was designed and manufactured. A 3 HP conventional lathe was used to provide rotary movement, and a hydraulic pressure system that applies axial force through a simple effect cylinder was designed to generate friction to obtain the union between the base materials.

Resumen

La soldadura de materiales disímiles hace que los procesos de soldadura convencional no sean factibles de ser utilizados. La soldadura por fricción, por otro lado, ha demostrado ser una tecnología prometedora capaz de unir materiales sin que la temperatura supere su punto de fusión. Sin embargo, la obtención de las propiedades mecánicas de la junta soldada con características similares a los materiales base sigue siendo un desafío. En el desarrollo de este trabajo se diseñó y fabricó un equipo de soldadura por fricción rotatoria con asistencia láser. Para proporcionar el movimiento rotatorio se empleó un torno convencional de 3 HP de potencia y para generar fricción se diseñó un sistema hidráulico de presión el cual aplica fuerza axial mediante un cilindro de simple efecto para obtener la unión entre los materiales base.

^{1,*}Departamento de Ingeniería Mecánica y Metalúrgica, Escuela de Ingeniería, Pontificia Universidad Católica de Chile, Av. Vicuña Mackenna 4860, Macul, Santiago, Chile. Corresponding author : gobarrionuevo@uc.cl

²Carrera de Tecnología Superior en Mecánica Automotriz, Instituto Superior Tecnológico Ciudad de Valencia (ISTCV), Quevedo, Ecuador

³Centro de Investigación en Nanotecnología y Materiales Avanzados (CIEN-UC), Av. Vicuña Mackenna, 4860, Macul, Santiago, Chile.

Suggested citation: Mollo, J. L.; Ramos-Grez, J. A. and Barrionuevo, G. O. "Design and construction of a friction welding equipment with laser assistance for the joint of AISI 1045 steel and aluminum 2017-T4 shafts," *Ingenius, Revista de Ciencia y Tecnología*, N.º 27, pp. 74-84, 2022, doi: <https://doi.org/10.17163/ings.n27.2022.07>.

In the implemented equipment, joints of AISI 1045 steel and 2017-T6 aluminum shafts were made. The welded joints were metallurgically evaluated, emphasizing on the chemical composition at the weld interface. For microstructure characterization, scanning electron microscopy (SEM), energy dispersion spectroscopy (EDS), and glow discharge optical emission spectrometry (GDOES) were used to measure the initial composition of the welded materials. The results obtained show an adequate joint between the base materials, denoting the usefulness of the equipment manufactured for the union of dissimilar materials.

Keywords: Steel, Aluminum, Laser, Dissimilar materials, Microstructure, Friction welding

En el equipo implementado se realizaron uniones de ejes de acero AISI 1045 con aluminio 2017-T6; las uniones soldadas se evaluaron metalúrgicamente, haciendo hincapié en la composición química en la interfaz de la soldadura. Para la caracterización de la microestructura se empleó microscopía electrónica de barrido (SEM), espectroscopía de dispersión de energía (EDS) y espectrometría de emisión óptica de descarga luminiscente (GDOES) para medir la composición inicial de los materiales que se soldaron. Los resultados obtenidos muestran una adecuada unión entre los materiales base, denotando la utilidad del equipo fabricado para la unión de materiales disímiles.

Palabras clave: acero, aluminio, láser, materiales disímiles, microestructura, soldadura por fricción

1. Introduction

The processes for joining metals have become an essential need for different industries related to metallurgy and welding. Depending on the sector, the appropriate selection of materials and procedures, together with security and quality standards, are essential aspects in the engineering industry [1]. When it is required to join materials with different characteristics, conventional fusion welding is unfeasible due to its metallurgic limitations. At present, conventional processes are not enough due to the difference between their melting points that generate intermetallic compounds of fragile features which are not beneficial at all for the welded joint [2]. Based on this issue, solid-state welding has been a promising joining process, in which two working pieces are joined under pressure, generating heat due to friction at temperatures below the melting point of the base materials [3]. Such friction welding (FW) has been an alternative solid-state joining method, since it produces a coalescence of materials under a compression force between two working pieces that rotate or move in contact producing heat and plastically displacing the material until creating a contact interface [4]. The weld metal, the flux and the protection gas are not necessary in this process, due to its simplicity. The process stated under the base of academic studies, has placed it among one of the best for the series production of joints in dissimilar materials [5]. For this reason, the FW process is used in the automotive, aeronautic, oil and electric industries, among others.

Joining steels with other materials in friction welding processes may have unexpected phase propagations, grain boundary corrosion or generation of delta and sigma ferrite phases in the welding interface. Therefore, some precautions have been considered, such as determining the variables with respect to thermal treatments, increasing welding velocity, because in this manner it will be achieved a certain homogeneity in the temperature distribution in the two components [6]. Under this context, obtaining welded joints with appropriate mechanical and metallurgic properties would contribute to the increasing interest in a broad range of industrial applications. Manufacturing components in the transportation and aeronautic industry, require welded cylindrical elements with good mechanical properties, low specific weight and good resistance to corrosion. Concretely, introducing steel and aluminum pieces in rotating systems and in steel structures require the development of reliable, efficient and economic joining processes. Through the application of a laser beam it might be possible to optimize the welding quality in a conventional FW process. Li, Yu, Li, Zhang and Wang [7] state that, during the conventional FW process, heat generation is mainly determined by the rotation speed, the friction pressure and the friction time. Thus, heating energy is very

limited, especially for welding slim axes.

The weld joint of the rotary friction welding process is the most important part and must be analyzed, characterized by a narrow heat affected zone (HAZ), presence of plastically deformed material around the welding (flash) and absence of a melted zone. Taban, Gould and Lippold [8] made joints between shafts of a 6061-T6 aluminum and AISI 1018 steel alloy, using rotational speeds up to 4200 rpm, friction pressure of 23 MPa, friction time of 1 s, forging times of 5 s and forging pressure of 60 MPa. Results showed a tensile strength of 250 MPa with failures in the plastic zone due to the existence of an interface with Al-Fe intermetallic compound, with a thickness of 250 nm related to the Fe_2Al_5 phases that are formed at temperatures above 1200 °C [9]. Handa and Chawla [10] adapted a conventional lathe with a pressure and brake system to create a RFW machine. The authors found that the maximum tensile strength and the impact resistance are acceptable at a rotational speed of 1250 rpm with an axial pressure of 120 MPa, for AISI 1021 steel welded joints with a diameter of 20 mm. On the other hand, Luo *et al.* [11] developed a method for joining a shock absorber and its rod, with the purpose of reducing the welding burrs. In this way they determined that, with an appropriate selection of parameters, the friction welding process is very effective for this type of applications, as opposed to conventional methods, because the obtained microstructure shows more uniform grains in the absence of phase change, which does not happen under fusion welding processes.

The main advantages of the CDFW process are the material saving, the short production time and the possibility of welding dissimilar materials. At present it is used for manufacturing elements in the automotive industry such as valves, gears, half shafts, turbo fan shafts, connections, pistons, etc. Ferrous and non-ferrous alloys are used to manufacture such elements [12]. Due to its versatility, friction welding has a generalized industrial use as a mass production process for joining materials [5]. However, to make dissimilar joints, the FW process requires alternative preheating methods with the purpose of providing better properties to the welded materials. For this reason, a rotary friction welding equipment was built during the development of this work, in which a preheating through laser is also applied to accelerate the process and improve coupling between base materials.

The operating principle for this experiment is illustrated in Figure 1, which describes the stages of the laser-assisted experiment in its design stage. In the development carried out, ω represents the rotational velocity in the left end, F_1 the friction force and F_2 the forging force. For this configuration, a laser beam acts on one of the materials, increasing its temperature before the rotary friction welding (RFW) process starts.

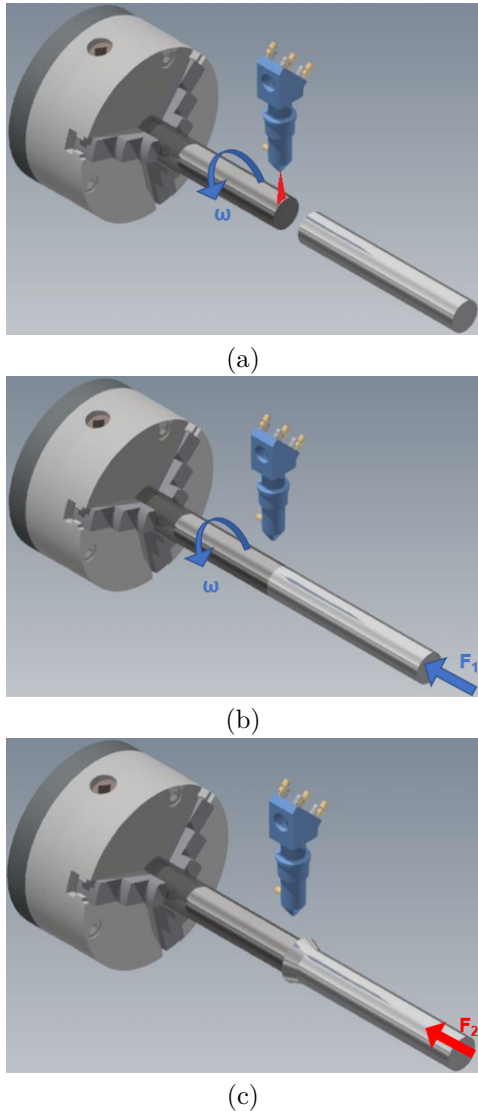


Figure 1. Stages of the laser-assisted friction welding process. a) Rotation of the steel shaft and laser activation. b) End of the laser application and start of the friction process through the application of the F_1 force. c) Suspension of the rotation and application of the forging axial force [13]

2. Materials and methods

An extensive literature review was conducted for the design process, identifying publications that present rotary friction welding known as Continuous drive friction welding [14–19]. Two essential mechanisms are identified in this process: one of rotation and another one of pressure. To move the shaft, it has been chosen a 3 HP conventional lathe, with a rotational velocity of 2000 rpm and a distance of 1000 mm between centers. Whereas for the friction and forging system, it was designed a hydraulically operated pressure system which enables making the friction joints at various pressure levels. The pressure mechanism consists of a hydraulic

system with a capacity of 5 tons, driven by a 300 c.c. hydraulic pump. The pressure mechanism also has a manometer that enables visualizing the friction and forging pressures.

For designing the pressure mechanism (Figure 2), a pressure counterpoint was coupled to the lathe, the design was carried out in the 3D Autodesk Inventor design software. Materials were used according to the stress degree to be withstood in the welding process. The structure of the device is built in AISI 1020 steel, while AISI 1045 and AISI 4120 steels were used for the parts that will receive a higher stress such as the nozzle fitting, the vibration damping block and the mounting flange, respectively. Figure 2a shows the designed counterpoint. Using Computer Assisted Engineering (CAE), the parts of the system were subject to a 1000 kg force to verify the maximum stress and its deformation in the shafts. The maximum deformation on the X axis, with a value of 0.1282 mm, may be observed in Figure 2b; this value is acceptable for the weld joints to be concentric and of quality.

For hydraulic design it was considered that the maximum force between test tubes is 1000 kg, according to the research conducted in [20]. The force established will enable making welding in steel or aluminum shafts with diameters up to 20 mm. An experimental test was conducted using a universal compression test machine to determine the hydraulic pressure. Applying pressure with the hydraulic piston and measuring the maximum force attained, it is obtained a pressure value that enables establishing the capacities of the system. Table 1 presents a pressure analysis for each pressure value in the cylinder.

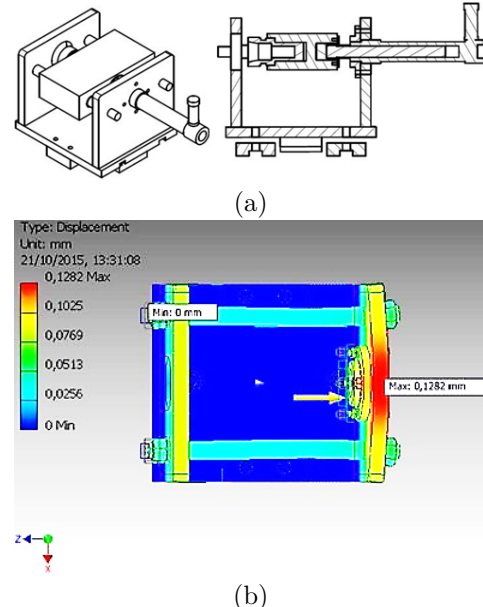


Figure 2. Design of the hydraulic pressure system, a) Computer assisted design, b) simulation of the maximum displacement

Table 1. Test pressures

Cylinder pressure (MPa)	Forced applied (kg)	Displacement (mm)
25,4	254	0,93
52	520	1,27
100	1000	1,79
149,9	1499	2,21
200,4	2004	2,62
624,4	6244	5,17

A CO₂ laser equipment (Oerlikon OPL3500) with a power of 3.5 kW, a wavelength of 10.6 μm and TEM00 (Figure 3) was used as heat source. Preheating is applied using this equipment so that the joint between the base materials is more efficient according to the results reported in the literature [21–27].

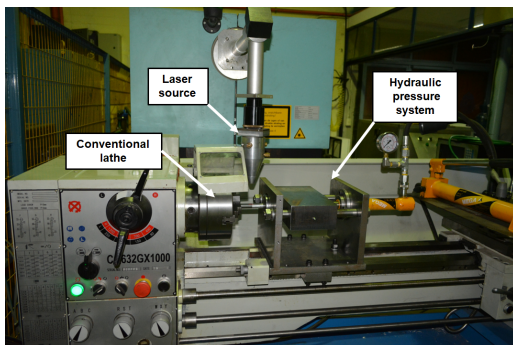


Figure 3. Laser-assisted friction welding (LAFW) equipment

The friction welding process was made on AISI 1045 shafts and 2017-T4 aluminum shafts, each with a diameter of 15 mm and a length of 180 mm. The nominal chemical compositions of the base materials are shown in Table 2. The mechanical properties of the base materials are presented in Table 3.

Table 2. Chemical composition of the base materials

Material	Elements (wt %)			
	Fe	C	Mn	Si
AISI 1045	98.41	0.40	0.72	0.22
	Cu	Al	P	S
AA 2017	0.13	0.02	0.01	0.01
	Al	Cu	Mg	Mn
AA 2017	92.92	4.25	1.58	0.84
	Fe	Zn	Cr	Si
	0.34	0.04	0.01	0.002

Table 3. Mechanical properties of the base materials

Material	Shear stress (MPa)	Creep stress (MPa)	Hardness (HV)
AISI 1045	617-680	330-392	260-330
AA 2017	370-420	215-260	105-120

The joining process consists of preheating the steel shaft for 40 seconds; the friction process starts when a rotational velocity between 1600 and 1800 rpm is reached, then the axial friction pressure is applied (14/21 MPa) through the hydraulic mechanism for 60 seconds, until achieving the forging. At last, a forging pressure (42.1 MPa) was applied for 40 seconds. These constant parameter values were chosen after various preliminary tests, in which it was found that these were the optimal values with respect to the capacity of the hardware used (Figure 4).

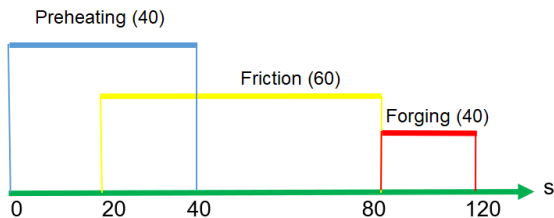


Figure 4. Parameters of the welding process

Where, for the time of laser preheating the pressure, $P = 0$ MPa. Afterwards for the friction time, the friction pressure $P_f = 14$ and 21 MPa. At last, at forging time the forging pressure increases to $P_u = 42.1$ MPa.

For macro and microstructural evaluation, 12 specimens obtained with the laser-assisted welding process were analyzed. The cross sections of the welded joints were subject to a metallographic preparation of coarse polishing with 200, 400, 600, 800 sandpapers, up to a grain sandpaper 1000 according to the ASTM E407 standard. It was applied a fine polishing using alumina with an average grain diameter of 0.04 μm and a diamond paste abrasive with a diameter of 0.01 μm to prevent irregularities on the sample surface. The equipment used to observe the microstructure is a MEIJI microscope model IM 7200 with an amplification up to 100x, 500x y 1000x.

With the purpose of visualizing the phases present and the grain size, a chemical attack was carried out on the steel through immersion for 10 seconds in a Nital solution (alcohol at 95 % and HNO₃ nitric acid in 5 ml). For the aluminum component, a swab was impregnated for 15 seconds with a hydrofluoric acid solution (1 ml of hydrogen fluoride HF and 200 ml of H₂O). The measurement of the grain size was carried out according to the ASTM E112 standard using the

intercept method for all cases. At last, a comparison was made between the conventional FW process and the LAFW process developed by the authors.

3. Results and discussion

During the welding process it is observed the application of the laser to the steel, and after the application of friction and forging a flash is formed around the aluminum shaft (Figure 5). The formation of the flash is mainly influenced by the characteristics of the material added to the friction pressure, which produces a more significant deformation, causing a larger effect of the flash due to the higher mechanical pressure [20].

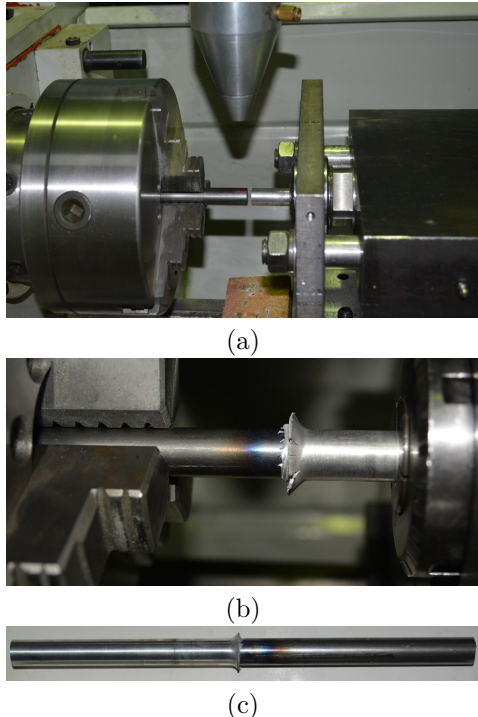


Figure 5. Welding process. a) Application of the laser on the steel shaft. b) Formation of the flash in the aluminum shaft. c) Welded test tube

In general, the aspect of the welded joint for the conditions established is symmetrical, the friction pressure mainly has influence on a flash effect that generally occurs in the aluminum side [8]. A larger mechanical pressure leads to a greater deformation of the material which in turn produces a larger flash effect (Figure 6).



Figure 6. Welded test tubes, where it may be observed different configurations of the flash on the aluminum shaft

The joint between aluminum and steel starts from the outer region and moves towards the center. The joint shown in Figure 7a presents a homogeneous joint, due to the additional heat supplied by the laser which promotes the homogenization of the material enabling the fusion of both materials [14]. To determine the quality of the joint it is necessary to analyze the microstructure through the chemical attack, to verify the deformation of the aluminum in the steel (Figure 7b).



Figure 7. Cross section – Micrograph of the steel-aluminum joint 500x

For steel-aluminum joints produced through friction welding, it is known that there are four zones defined from the ends towards the center: non-deformed zone (NDZ), heat affected zone (HAZ), thermo-mechanically affected zone (TMAZ) and Fe-Al reaction

or interface layer. In the case of the steel, the NDZ presents a matrix constituted by approximately 39.36 % of ferrite and 60.64 % of perlite. The matrix has a 0.45 % of carbon and an ASTM 6 grain size, which corresponds to an AISI 1045 steel (Figure 8a). The HAZ shows a light grain refinement, similar to the ones obtained in [28]. The most critical microstructure zone is the TMAZ, which is characterized by a greater grain refinement, because there is a temperature increase and fast cooling. With respect to the aluminum, the NDZ presents a matrix constituted by approximately 93.85 % of aluminum and 6.15 % of copper. The matrix has an ASTM 10 grain size which corresponds to an AA 2017 aluminum (Figure 8b).

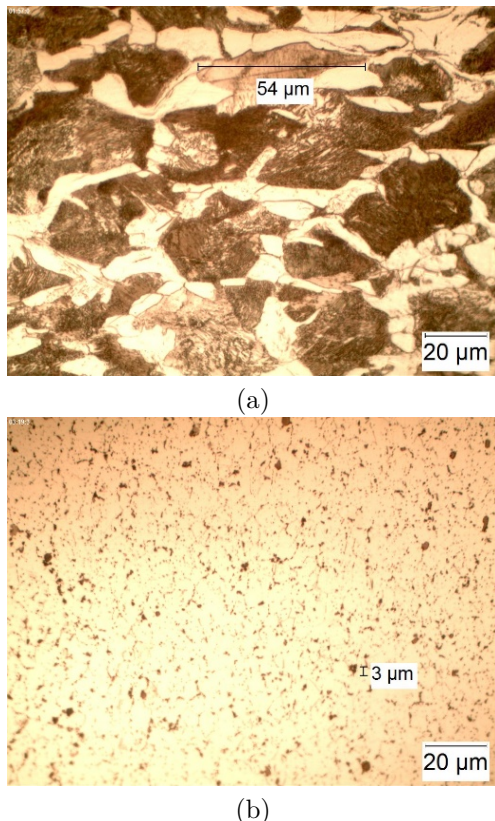


Figure 8. Optical microscopy at 10000x of the thermo mechanically affected zone a) Steel. b) Aluminum

The HAZ presents a grain refinement similar to the ones obtained in [29]. There is a greater thermo-mechanical deformation due to the fusion by friction since it is a material with a lower melting point than steel.

With respect to the laser-assisted TMAZ, it was analyzed at an amplification of 1000x as described in Figure 8a, and in Table 4 it may be observed the 53.31 % of the perlite matrix, and it also appears 46.49 % of non-circular ferrite due to the heating and fast cooling produced by friction pressure and laser assistance. The grain size is ASTM 6, with an average dimension of approximately 54 microns calculated through the intercept method. In Figure 8b there is a 94.56 % of

aluminum and 5.44 % of copper. There is grain size of ASTM 9 and a maximum diameter of three microns.

Table 4. Phases and elements present in the base materials

AISI 1045		
Perlite area	1 020 967,40	μm ²
Ferrite area	887 088,60	μm ²
Perlite %	53,51%	
Ferrite %	46,49%	
Total area	1 908 056	μm ²

AA 2017-T4		
Copper area	103 810,60	μm ²
Aluminum area	1 804 245,40	μm ²
Copper %	5,44%	
Aluminum %	94,56%	
Total area	1 908 056	μm ²

Figure 9 shows the analysis points for determining the chemical composition of each material by means of glow discharge optical emission spectrometry (GDOES), aluminum to the left and steel to the right, In the center there is the weld interface (point 3). The results obtained are presented in Table 5. It is clearly distinguished the larger concentration of aluminum (Al) around 82 %, copper (Cu) about 9 % and manganese (Mn) above 5 % for the 2017-T4 alloy. For the 1045 steel there is an iron (Fe) concentration greater than 97 %. Whereas in the interface the chemical composition is redistributed in 62 % Fe and 33 % Al, with smaller content of Cu and Mn.

To complement the microstructure analysis, Figure 10 shows an elementary mapping by means of energy dispersive spectroscopy (EDS). It may be observed the variation in the content of elements along the weld interface. In the upper part there is Fe at a greater concentration, identified by the red color corresponding to the 1045 steel alloy. In the lower part it is distinguished the Al in yellow color corresponding to the 2017-T4 alloy. It is also possible to distinguish a high concentration of Cu in the lower part and silicon (Si) to a lesser extent, in both the steel alloy and in the aluminum.

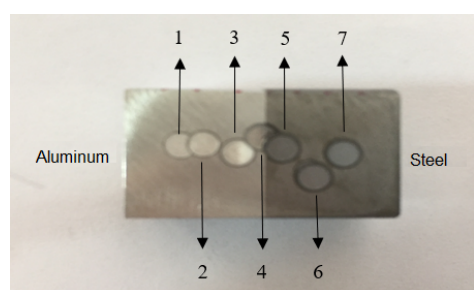


Figure 9. Glow discharge optical emission spectrometry, analysis points to determine elementary chemical composition

Table 5. Measurement of the chemical composition by means of GDOES at the points indicated

Point	Fe [%]	C [%]	Mn [%]	Si [%]	P [%]	S [%]	Ni [%]	Cu [%]	Al [%]	Zn [%]
1	0,78	0,131	5,671	0,184	0,321	0,6831	0,153	8,973	81,891	0,298
2	0,78	0,133	5,588	0,188	0,3017	0,7894	0,153	8,895	81,971	0,294
3	0,73	0,124	5,513	0,173	0,3363	0,8181	0,183	9,08	81,851	0,277
4	61,93	0,063	1,079	0,222	0,0465	0,0148	0,128	3,228	32,786	0,094
5	97,84	0,131	0,849	0,185	0,0138	0,0102	0,185	0,504	0,019	0,007
6	97,88	0,134	0,828	0,18	0,0134	0,0097	0,181	0,494	0,018	0,009
7	97,87	0,133	0,833	0,182	0,0128	0,0097	0,181	0,505	0,013	0,006

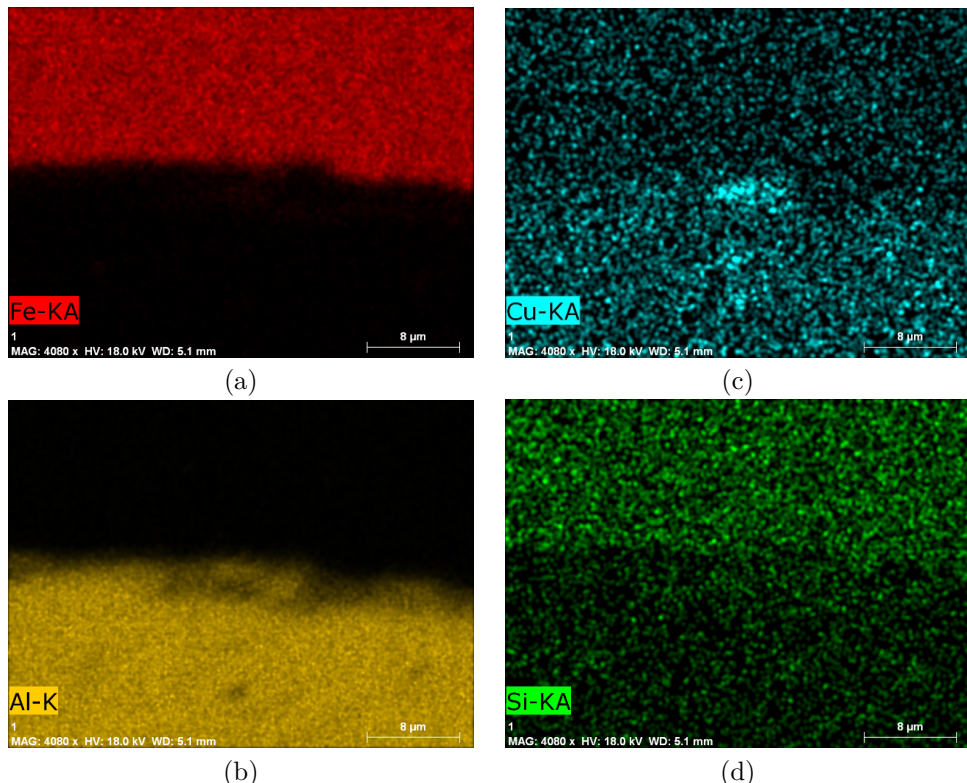


Figure 10. Energy dispersive spectroscopy (EDS) – Elementary mapping

4. Conclusions

A laser-assisted friction welding system was developed, where it may be controlled the rotational speed of the system through a frequency drive. The optimum speed chosen through experimental tests corresponds to a range between 1600 and 1800 rpm.

The developed hydraulic pressure system is capable of providing an axial force above 9800 N, enabling to make welding in steel-aluminum shafts with diameters up to 20 mm. The pressure range to generate friction and accelerate the welding process is in the range from 14 to 21 MPa.

The application of the laser beam on the steel shaft enables homogenizing the microstructure, which in

turn accelerates the welding process so that there is a larger weld interface between the steel and aluminum shafts, which have been verified in the microstructure analyses.

It was determined the grain size for each element, for the steel an average grain of ASTM 8 with a maximum diameter of 6 microns. For the aluminum, there is a grain size of ASTM 9 and a maximum diameter of 3 microns.

In the weld interface it was determined a decrease in iron (Fe) and aluminum (Al). The Fe decreases from 97.8 % to 61.9 %, whereas the aluminum goes from 81.9 % to 32.8 %. It could be also determined the existence of manganese, copper and silicon in smaller proportion than the base materials.

References

- [1] A. Handa and V. Chawla, "Experimental evaluation of mechanical properties of friction welded dissimilar steels under varying axial pressures," *Strojnický časopis - Journal of Mechanical Engineering*, vol. 66, no. 1, pp. 27–36, 2016. [Online]. Available: <https://doi.org/10.1515/scjme-2016-0008>
- [2] S. D. Meshram, T. Mohandas, and G. M. Reddy, "Friction welding of dissimilar pure metals," *Journal of Materials Processing Technology*, vol. 184, no. 1, pp. 330–337, 2007. [Online]. Available: <https://doi.org/10.1016/j.jmatprotec.2006.11.123>
- [3] W. Cai, G. Daehn, A. Vivek, J. Li, H. Khan, R. S. Mishra, and M. Komarasamy, "A State-of-the-Art Review on Solid-State Metal Joining," *Journal of Manufacturing Science and Engineering*, vol. 141, no. 3, p. 031012, 01 2019, 031012. [Online]. Available: <https://doi.org/10.1115/1.4041182>
- [4] P. Sathiya, S. Aravindan, and A. Noorul Haq, "Effect of friction welding parameters on mechanical and metallurgical properties of ferritic stainless steel," *The International Journal of Advanced Manufacturing Technology*, vol. 31, no. 11, pp. 1076–1082, Feb. 2007. [Online]. Available: <https://doi.org/10.1007/s00170-005-0285-5>
- [5] A. Hascalik and N. Orhan, "Effect of particle size on the friction welding of Al₂O₃ reinforced 6160 Al alloy composite and SAE 1020 steel," *Materials and Design*, vol. 28, no. 1, pp. 313–317, 2007. [Online]. Available: <https://doi.org/10.1016/j.matdes.2005.06.001>
- [6] N. Ozdemir, F. Sarsilmaz, and A. Hascalik, "Effect of rotational speed on the interface properties of friction-welded AISI 304L to 4340 steel," *Materials and Design*, vol. 28, no. 1, pp. 301–307, 2007. [Online]. Available: <http://dx.doi.org/10.1016/j.matdes.2005.06.011>
- [7] W.-Y. Li, M. Yu, J. Li, G. Zhang, and S. Wang, "Characterizations of 21-4N to 4Cr₉Si₂ stainless steel dissimilar joint bonded by electric-resistance-heat-aided friction welding," *Materials and Design*, vol. 30, no. 10, pp. 4230–4235, 2009. [Online]. Available: <https://doi.org/10.1016/j.matdes.2009.04.032>
- [8] E. Taban, J. E. Gould, and J. C. Lippold, "Dissimilar friction welding of 6061-t6 aluminum and aisi 1018 steel: Properties and microstructural characterization," *Materials and Design (1980-2015)*, vol. 31, no. 5, pp. 2305–2311, 2010. [Online]. Available: <https://doi.org/10.1016/j.matdes.2009.12.010>
- [9] S. Fukumoto, H. Tsubakino, K. Okita, M. Ariyoshi, and T. Tomita, "Amorphization by friction welding between 5052 aluminum alloy and 304 stainless steel," *Scripta Materialia*, vol. 42, no. 8, pp. 807–812, 2000. [Online]. Available: [https://doi.org/10.1016/S1359-6462\(00\)00299-2](https://doi.org/10.1016/S1359-6462(00)00299-2)
- [10] A. M. I. T. HANNA and V. I. K. A. S. CHAWLA, "Experimental study of mechanical properties of friction welded aisi 1021 steels," *Sadhana*, vol. 38, no. 6, pp. 1407–1419, Dec. 2013. [Online]. Available: <https://doi.org/10.1007/s12046-013-0181-x>
- [11] J. Luo, Y. H. Ye, J. J. Xu, J. Y. Luo, S. M. Chen, X. C. Wang, and K. W. Liu, "A new mixed-integrated approach to control welded flashes forming process of damping-tube-gland in continuous drive friction welding," *Materials and Design*, vol. 30, no. 2, pp. 353–358, 2009. [Online]. Available: <https://doi.org/10.1016/j.matdes.2008.04.075>
- [12] S. Celik and I. Ersozlu, "Investigation of the mechanical properties and microstructure of friction welded joints between AISI 4140 and AISI 1050 steels," *Materials & Design*, vol. 30, no. 4, pp. 970–976, 2009. [Online]. Available: <https://doi.org/10.1016/j.matdes.2008.06.070>
- [13] J. L. Mullo, J. A. Ramos-Grez, and G. O. Barriónuevo, "Effect of laser heat treatment on the mechanical performance and microstructural evolution of AISI 1045 steel-2017-T4 aluminum alloy joints during rotary friction welding," *Journal of Materials Engineering and Performance*, vol. 30, no. 4, pp. 2617–2631, Apr. 2021. [Online]. Available: <https://doi.org/10.1007/s11665-021-05614-6>
- [14] G. L. Wang, J. L. Li, W. L. Wang, J. T. Xiong, and F. S. Zhang, "Rotary friction welding on dissimilar metals of aluminum and brass by using pre-heating method," *The International Journal of Advanced Manufacturing Technology*, vol. 99, no. 5, pp. 1293–1300, Nov. 2018. [Online]. Available: <https://doi.org/10.1007/s00170-018-2572-y>
- [15] S. Celik and I. Ersozlu, "Investigation of the mechanical properties and microstructure of friction welded joints between AISI 4140 and AISI 1050 steels," *Materials and Design*, vol. 30, no. 4, pp. 970–976, 2009. [Online]. Available: <https://doi.org/10.1016/j.matdes.2008.06.070>
- [16] W. Li, A. Vairis, M. Preuss, and T. Ma, "Linear and rotary friction welding review," *International Materials Reviews*, vol. 61, no. 2, pp. 71–100, 2016. [Online]. Available: <https://doi.org/10.1080/09506608.2015.1109214>

- [17] P. Ferro, Y. Wei, and F. Sun, "Microstructures and mechanical properties of Al/Fe and Cu/Fe joints by continuous drive friction welding," *Advances in Materials Science and Engineering*, vol. 2018, p. 2809356, Jun. 2018. [Online]. Available: <https://doi.org/10.1155/2018/2809356>
- [18] O. D. Hincapié, J. A. Salazar, J. J. Restrepo, J. A. Graciano-Uribe, and E. A. Torres, "Weldability of aluminum-steel joints using continuous drive friction welding process, without the presence of intermetallic compounds," *Engineering Journal*, vol. 24, no. 1, pp. 129–144, 2020. [Online]. Available: <https://doi.org/10.4186/ej.2020.24.1.129>
- [19] X. Li, J. Li, F. Jin, J. Xiong, and F. Zhang, "Effect of rotation speed on friction behavior of rotary friction welding of aa6061-t6 aluminum alloy," *Welding in the World*, vol. 62, no. 5, pp. 923–930, Sep. 2018. [Online]. Available: <https://doi.org/10.1007/s40194-018-0601-y>
- [20] E. Taban, J. E. Gould, and J. C. Lippold, "Dissimilar friction welding of 6061-t6 aluminum and aisi 1018 steel: Properties and microstructural characterization," *Materials and Design (1980-2015)*, vol. 31, no. 5, pp. 2305–2311, 2010. [Online]. Available: <https://doi.org/10.1016/j.matdes.2009.12.010>
- [21] X. Fei, X. Jin, N. Peng, Y. Ye, S. Wu, and H. Dai, "Effects of filling material and laser power on the formation of intermetallic compounds during laser-assisted friction stir butt welding of steel and aluminum alloys," *Applied Physics A*, vol. 122, no. 11, p. 936, Oct. 2016. [Online]. Available: <https://doi.org/10.1007/s00339-016-0462-4>
- [22] T. Wada, Y. Morisada, Y. Sun, H. Fujii, Y. Kawahito, M. Matsushita, and R. Ikeda, "Friction stir welding of medium carbon steel with laser-preheating," *ISIJ International*, vol. 60, no. 1, pp. 153–159, 2020. [Online]. Available: <https://doi.org/10.2355/isijinternational.ISIJINT-2019-394>
- [23] X. Fei, J. Li, W. Yao, and L. Jin, "Study of temperature on microstructure and mechanical properties on fe/al joint in laser-assisted friction stir welding," *AIP Advances*, vol. 8, no. 7, p. 075214, 2018. [Online]. Available: <https://doi.org/10.1063/1.5039417>
- [24] M. Kutsuna, N. Yamagami, M. J. Rathod, and H. Y. A. Ammar, "Laser roll welding for joining of low-carbon steels to aluminium alloys," *Welding International*, vol. 20, no. 6, pp. 446–456, 2006. [Online]. Available: <https://doi.org/10.1533/wint.2006.3599>
- [25] Q. Guan, J. Long, P. Yu, S. Jiang, W. Huang, and J. Zhou, "Effect of steel to aluminum laser welding parameters on mechanical properties of weld beads," *Optics and Laser Technology*, vol. 111, pp. 387–394, 2019. [Online]. Available: <https://doi.org/10.1016/j.optlastec.2018.09.060>
- [26] S. L. Campanelli, G. Casalino, C. Casavola, and V. Moramarco, "Analysis and comparison of friction stir welding and laser assisted friction stir welding of aluminum alloy," *Materials (Basel, Switzerland)*, vol. 6, pp. 5923–5941, Dec 2013. [Online]. Available: <https://doi.org/10.3390/ma6125923>
- [27] M. Merklein and A. Giera, "Laser assisted friction stir welding of drawable steel-aluminium tailored hybrids," *International Journal of Material Forming*, vol. 1, no. 1, pp. 1299–1302, Apr. 2008. [Online]. Available: <https://doi.org/10.1007/s12289-008-0141-x>
- [28] M. Yilmaz, M. Çöl, and M. Acet, "Interface properties of aluminum/steel friction-welded components," *Materials Characterization*, vol. 49, no. 5, pp. 421–429, 2002. [Online]. Available: [https://doi.org/10.1016/S1044-5803\(03\)00051-2](https://doi.org/10.1016/S1044-5803(03)00051-2)
- [29] N. R. J. Hynes, P. Nagaraj, and J. A. J. Sujana, "Investigation on joining of aluminum and mild steel by friction stud welding," *Materials and Manufacturing Processes*, vol. 27, no. 12, pp. 1409–1413, 2012. [Online]. Available: <https://doi.org/10.1080/10426914.2012.667894>